DOI:

# Cold gas roll control for a 30kg experimental rocket

*Florian COURTEVILLE, Enrico Mario GIOVANARDI and Elouan PETERAU*
*SUPAERO SPACE SECTION*
*04 Avenue Edouard Belin TOULOUSE,*
flo.courteville@gmail.com · enricom.giovanardi@gmail.com ·
Elouan.PETEREAU@student.isae-supaero.fr

## Abstract

This document describes the realisation and test of a cold gas roll control for a 30kg rocket. A pneumatic circuit provides thrust with pairs of nozzles and a mechanical system integrate it into the rocket and uses extendable arm to increase the lever arm. The system is controlled and stabilised by a non-linear control law based on a Schmitt trigger, tuned to reach the desired performance in terms of roll angle and to limit the activation frequency of the valves letting air through the nozzles. An custom made electronic card implements the control law by activating the solenoid valves using mosfets. Some test were conducted on test bench to observe the capabilities of the system.

## 1. Introduction

PERSEUS is a European project led by students and operated by CNES, the French space agency. The aim is to allow students to engage in space related activities and gain valuable experience that will train them prior to beginning their professional activities in the sector. Within the framework of PERSEUS, SUPAERO SPACE SECTION works since September 2021 on the development of a cold gas roll control system for experimental rockets. Those rockets are crafted with the collaboration of other French engineering schools. The first version of the system was launched on the rocket CERES at the 2022 C'Space. A refined version of the system will be launched on the 30kg experimental rocket SERENDIPITY at the 2023 C'Space. This paper describes the development of the roll control system that can be broken down in four parts: pneumatic, mechanical structure electronics and control. The main challenges arise from two aspects. On one side, the difficulty of building a pneumatic system capable of providing an important roll control moment with pieces off-the-shelf. On the other side, the non linearity of the rocket dynamics and of the cold gas actuators, leading to a non-linear control law with adaptive gains. A third but not less important aspect concerns the implementation of the law in the electronic card: without a proper scheduling of recurrent operations and the treatment of the navigation data, the control could not be put in place.

Copyright © 2023 by Florian COURTEVILLE. Posted on line by the EUCASS association with permission.

## 2. Pneumatic

To provide the moment needed to control the system, a pneumatic system is put in place to provide thrust with two pairs of nozzles blowing compressed air in opposed directions. The pneumatic system is also used in parallel to deploy the mechanical system. To maximise the thrust, convergent-divergent nozzles where designed and made.

### 2.1 Architecture

Compressed air up to 200 bar is stored inside a paintball air tank and is decompressed to 5 bar through a regulator. A fill nipple associated with a check valve is screwed in parallel of the regulator to refill the system. Then four 5/3 solenoid valves are connected to the regulator and each nozzle are connected to a pair of valves. A fifth 5/3 solenoid valve is also connected and supply 2 double acting cylinders, with flow control valves inserted at each outlet. Finally, the external pilot air supplies of the solenoid valves are connected to the main circuit with check valves. Flexible hose and push in fitting are used to connect the low pressure elements.

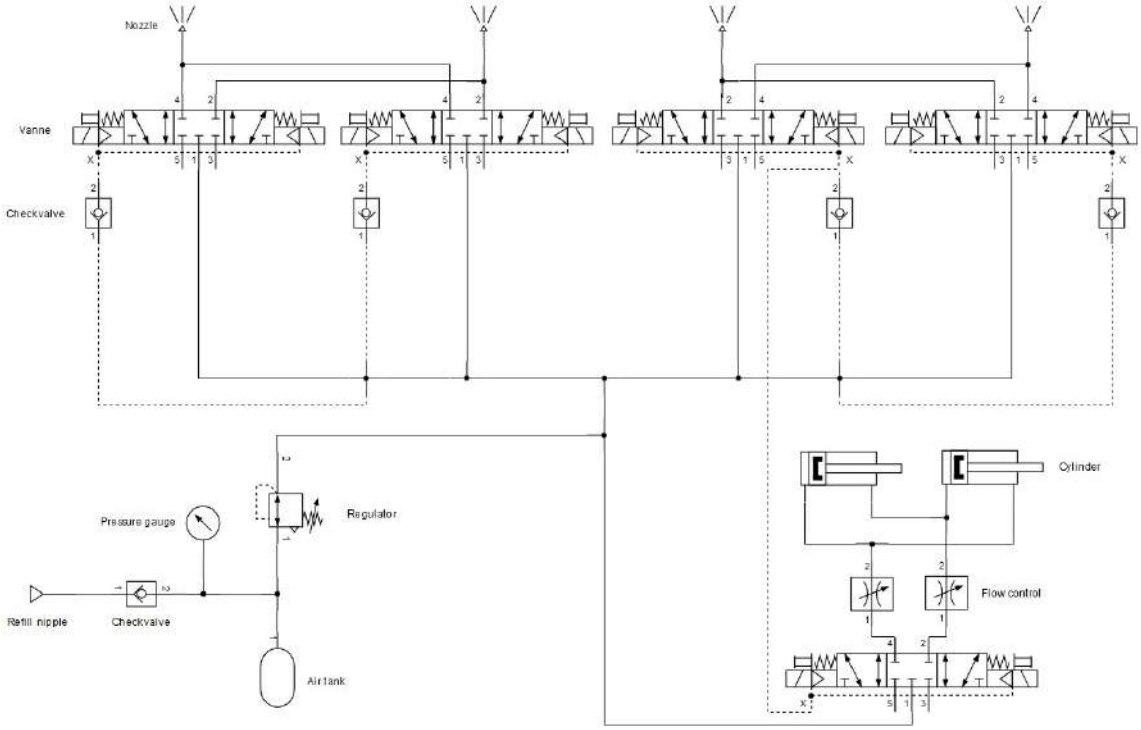


Figure 1: Pneumatic circuit

### 2.2 Nozzle

#### 2.2.1 Design

The flow inside the nozzle is assumed quasi-mono-dimensional and the compressed air is assimilated as an ideal gas with adiabatic index $\gamma$ and specific gas constant $r$. By using those hypotheses, total temperature $T_t$ and total pressure $P_t$, the reduced flow rate $\dot{m}_r$ and the invariant $\Sigma$ are established in eq. 1 and eq. 2.

$$\dot{m}_r = \dot{m}\frac{\sqrt{rT_t}}{AP_t} = \sqrt{\gamma}M(1+\frac{\gamma+1}{2}M^2)^{-\frac{\gamma+1}{2(\gamma-1)}} \tag{1}$$

$$\Sigma = \frac{m_r\dot{(}1)}{m_r\dot{(}M)} = \frac{1}{M}[\frac{2}{\gamma+1}(1+\frac{\gamma-1}{2}M^2)]^{\frac{\gamma+1}{2(\gamma-1)}} \tag{2}$$

These quantities are depending only on the Mach number $M$. Moreover, as long as the flow is isentropic, $P_t$ is constant along the nozzle. It allows the calculation of the exit Mach $M_e$ through eq. 3 by fixing the static exit pressure $P$ at the atmospheric pressure to maximise the thrust. It also allows a new expression of $\Sigma$ presented in eq. 4 with $A$ the section area and $A_c$ the section area of the throat where Mach equal 1, which can be calculated by using eq. 1 and depends on the mass flow rate ($\dot{m}$). The exit section of the nozzle is so obtained by calculating $\Sigma$ at $M_e$.

$$\frac{P_t}{P} = (1 + \frac{\gamma - 1}{2} M^2)^{\frac{\gamma}{\gamma - 1}} \tag{3}$$

$$\Sigma(M) = \frac{A}{A_c} \tag{4}$$

It can be noted that, according to eq. 1, at fixed $P_t$, $T_t$ and $A$, $\dot{(m)}$ can not exceed the value for Mach equal 1, which means that the smallest section of the air circuit imposes a limitation of the mass flow rate. So, when designing the rest of the circuit, special care is made to be sure than the smallest section of the circuit is the throat of the nozzle, which imposes the desired mass flow rate.

#### 2.2.2 Manufacture

According to the maximum flow rate capabilities of the potential pneumatic elements present on the market, a mass flow rate of 0.04 kg/s is chosen to go through each nozzle. With a pressure of 5 bar and a temperature of 297K and with the method of calculation described above, the nozzles are made with a throat of a 6.5 mm diameter and an exit of 8 mm diameter for an exit thrust of 19.2 N . They are made into an inox tube which is threaded on the outside in G 1/4.

### 2.3 Element choices

When choosing the elements for the circuit, some criteria are more important in the case of this system. Naturally, all elements must be the lightest due to the limitation in mass of the system. Also, they must be certified to withstand two time the pressure of the circuit (in our case 10 bar for the low pressure circuit and 400 bar for the high pressure circuit). Those two criteria already reduce a lot the choice of elements in the market. The refill system, the pilot air supply circuit and the cylinder circuit are chosen over those criteria. Regarding the nozzle circuit, it must allow a sufficient flow rate so that the nozzles are adapted and give the nominal force. For the flexible hose and push in fitting, the criterion is to have a minimum section bigger than the criteria discussed before. For the valves and the regulator, it is the $K_v$ that has to be large enough. This coefficient which gives an estimate of the flow rate depending on the inlet and outlet pressure. Regulator's data also provide a flow curve to have a better idea of the capabilities. Finally, valves also must have a response time fast enough so that the control law is effective.

### 2.4 Operation

The system provides the moment by activating the valves so as each nozzle of a pair receive air from two valves. It also can be passivated without creating a force or moment by supplying each of the four nozzles with one valve only. For the cylinders, one side of the fifth valve is used to setup the system before launch, and the other one is used to release and damp the release of the mechanical system.

## 3. Mechanic

To integrate the pneumatic system in the rocket, a mechanical system is built around it to support it during the flight. Moreover, due to a limitation of the nozzles' thrust, two extendable arms are built to increase the lever arm of the nozzles from 100 mm to 293 mm.

### 3.1 Main architecture

Two rings, one above and the other under the air tank, connected with two threaded rods and screwed in the rocket external structure maintain in place the pneumatic system and receive stresses during the flight. The fourth main valves are screwed on two plates fixed on the rod, and the release cylinders are screwed to both plates and top ring to ensure stability. The fifth valve is fixed directly on one rod on top of the system. The damp cylinders are fixed on the rods between the two rings. The arms are fixed under the bottom ring with hinges.

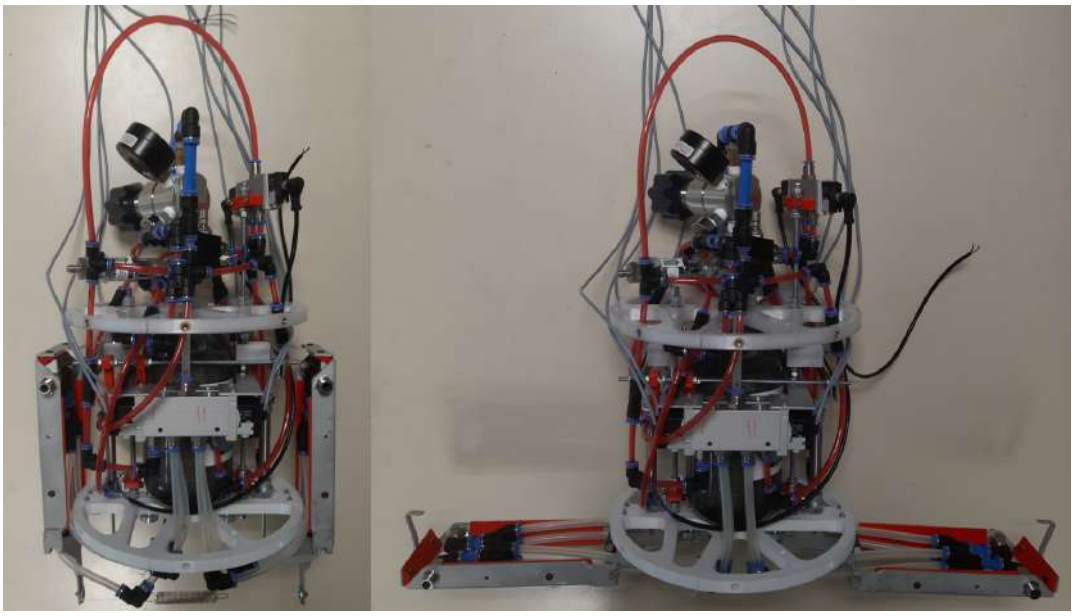

Figure 2: Unextended and extended system

### 3.2 Extension mechanism

#### 3.2.1 Arms

The arms are made from folded and cut aluminium sheet in order to be easy to produce. At the front two holes are present to screw the nozzles in and a hook to keep the arm unextended during the take off. The hinge is fixed at the middle of the arm and at the back, a metal coin is attached, which allow a magnet attached at the bottom ring to catch and maintain the arm when extended. Small holes are made on the side to attach canard, as well as the middle of the arm was cut down to reduce the aerodynamic drag. Finally, inox brackets are welded at the centre angles so that the arms can withstand the stress when deployed.

#### 3.2.2 Hold and release mechanism

As the estimated maximum velocity of the rocket is 234 m/s, two canards are added on the rocket above the arms so that the arms won't be in the direct air flow during the take-off. To maintain the arms close to the rocket during this stage, two plate of metal around each hook prevent the arm to fall. The arms are released when the cylinders connected to the plate extend and release the hook. The tension of the tube and the wind then make the arms fall.

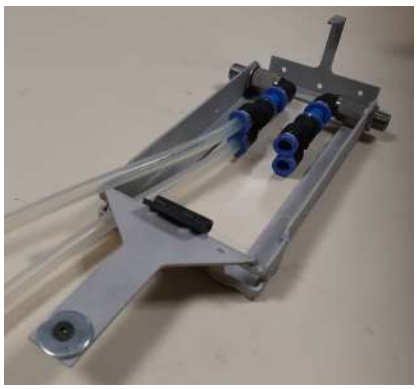

Figure 3: Picture of one arm

### 3.2.3 Damp and catch mechanism

The velocity $V$ of the rocket at the release will be 150 m/s when the arm will be extended. Equation eq. 5 give that the drag force D on one arm when extended are around 134 N. $\rho$ is the density of air, S is the area of the horizontal flat front face of the arm plus the planform area of the tubes exposed to the air flow. Is $C_D$ the drag coefficient, which is taken equal to 1.17 for both the flat area and the tubes.[1]

$$D = \frac{1}{2}\rho V^2 S C_D \tag{5}$$

To avoid any damage during the extension, the arms will fall against a plate supported by 2 cylinders that have to be fully retracted to have the arms extended. By limiting the flow rate at the outlet of the cylinder, the maximum speed of retractions can be limited, and shocks can be prevented. When fully deployed, arms will be hold against the bottom ring with 20kg magnets and metallic cables hooked to the front of the arms and to the rocket above the system will prevent the system to bend.

# 4. Electronics and software

## 4.1 Electronic system

To simplify the integration of the system with the whole rocket, a custom PCB board is used.
This PCB contains the following parts:

- The single board computer `Raspberry PI zero 2W` used to host the control software
- The Ethernet controller `ENC28J60` that allow the raspberry pi to have an Ethernet capability
- The `2N7000` mosfets used to control the 24V valves from the Raspberry 3.3V output voltage
- The opto-isolators used to separate the control part of the PCB board from the power part
- The DC/DC Converters that are giving the required output voltages to all the components (3.3V, 5V and 24V)
- The `SUB-D` connector used to access to all the 37 output and input signals of the board

Thanks to this, we only have one power input of 24V, which greatly simplify the integration with the rocket, and all the output connections are easily plug-able without the risk of inverting two cables.

On top of the 2 power inputs pins, the 4 Ethernet RX/TX pins, the 18 valves pins and the 2 passivation pins, the `SUB-D` connector also have 2 pins reserved for an on-off software switch and 2 pins for a signal led.
Additionally, even if it is not used, this board contain the possibility to control two servo motor using a `PWM` signal if required and have 6 pins reserved for this.

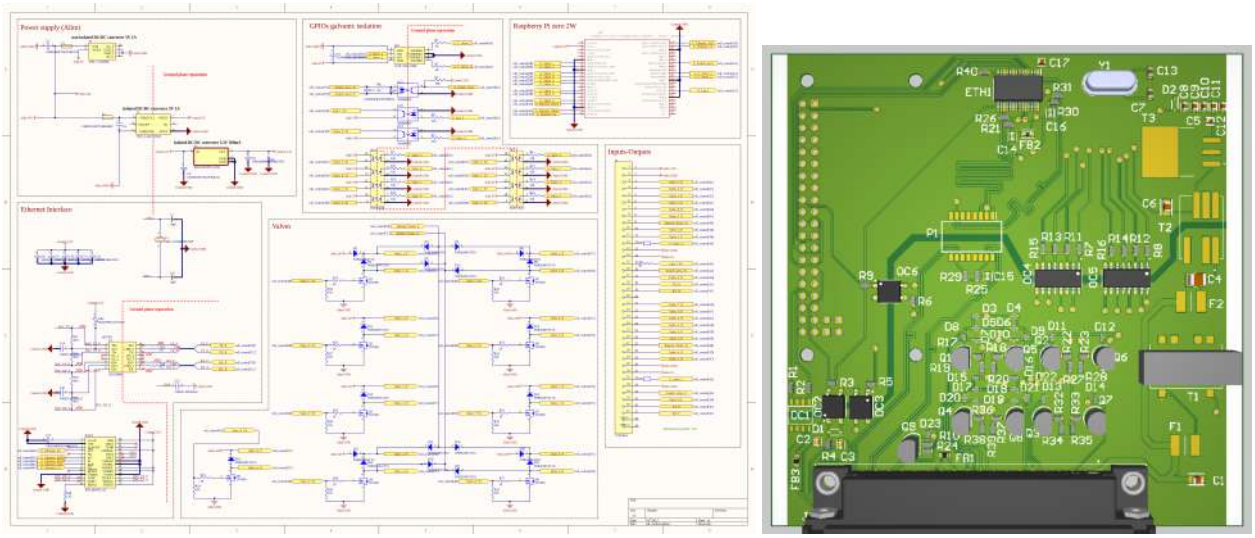

(a) Electronic schematic

(b) 3D view of the PCB

Figure 4: Screenshot of the board

## 4.2 Real time software

To ensure a complete preemption of the system and have an accurate update of the control law, a Debian 11 Operating system patched with `PREMPT_RT` is used on the Raspberry Pi. This allow to have access to the standard library of the C library like the threading, signal and mutex systems while ensuring that each task is run exactly when desired.

For the software, 3 different tasks, with a designated role each, are used. They are namely the `data_receiver`, the `period_manager` and the `roll_controller` tasks.

Firstly, since the system receive the rocket status, i.e. if the we had a liftoff or not, as well as all the IMU position data through an UDP socket across the Ethernet communication, a designed tasks have been defined to receive this data and parse it.
This task is named `data_receiver` and, when it receive a data on the socket, depending on it's type, it will do the following thing:

- If it is the liftoff signal, update the state global variable and start the roll control
- If it is an IMU data, store on a file the received data with the current time and if the roll control have started, send the data to the data FIFO queue

Additionally, an atomic global variable is used to keep track of the system state. This variable can either be updated by the `data_receiver` task or `period_manager` task and will also be written on the data log file.

Then, to allow the `period_manager` task to signal to the `roll_controller` task when the experience as changed or when to update the law and control the roll using the air flow, 4 event signals are used. There is 3 experience mode, one where nothing is controlled, one where the system stabilize the roll angle and one where the system will change the angle from +90° to −90° relative to the starting angle.
Now to bock the execution of the `period_manager` task until the liftoff, a binary semaphore is used and released by the `request_manager` task when it receive the liftoff message on the UDP socket.
Then after a defined amount of time it will change the experiment mode by sending one the signal defined above. The end of all the experiments is sent to the `data_receiver` using a flag signal to stop it from filling the data queue.

Finally, a task named `roll_controller` is used to update the control model and control the valves and thus the rocket roll. The model variables will be updated, by using the mean values of all the remaining data in the FIFO queue and this every 5ms after the task receive the signal from the `period_manager` task. Then, the valves will be opened to change the rocket x-angle accordingly to the current experience requirements.

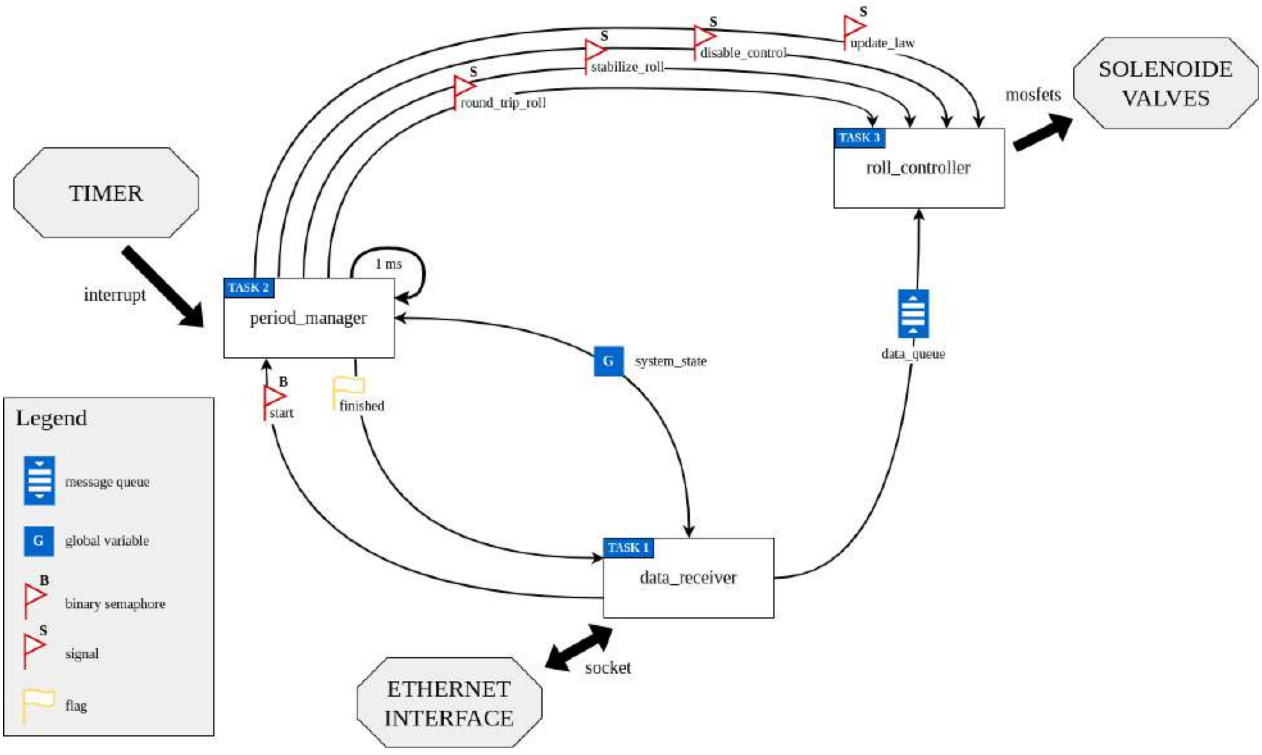


Figure 5: Diagram of the software architecture

## 5. Control and navigation

To control the roll angle of the rocket, a control law with adaptive gains is put in place, and an IMU is used to retrieve the necessary measurements. Then, the mission structure defines the guidance, represented by the reference roll angle to be tracked.

### 5.1 Physical system

The non-linearity of the aerodynamic forces and the rotational coupling of the rocket axes would make the conception of a robust control law hard. Thus, initial hypotheses are made:

- The rotation around the roll axis is decoupled, due to the slow pitch and yaw rotation during the flight of the rocket, supposed stable.
- The dynamics are evaluated at different velocity operating points, each of which define a linear system around such points.

According to the hypotheses, the following dynamics can be expressed as in eq. 6, where $I$ stands for the moment of inertia around the roll axis and $\phi$ for the roll angle. The external moments are then the aerodynamic one $M_{aero}$ and the control moment given by the cold gas thrusters $M_c$.

$$I\ddot{\phi} = M_{aero} + M_c \tag{6}$$

Two components of the aerodynamic force can be distinguished, a forcing component and a damping component. The first (represented by the aerodynamic coefficient $C_{l_0}$) depends on the misalignment of the centre of gravity or of the wings at the base of the rocket. The second one (represented by the positive aerodynamic coefficient $C_{l_p}$) is proportional to the roll angular velocity, with a factor depending on the diameter $d$ of the rocket. Both are generated by the presence of the wings and the overall moment coefficient $C_l$ and the aerodynamic moment can be expressed as follows:

$$C_l = C_{l_0} - C_{l_p}\dot{\phi}d/v \tag{7}$$

$$M_{aero} = \frac{1}{2}\rho v^2 C_l S\, d \tag{8}$$

It is clear how fixing the velocity $v$ of the rocket at a certain operating point helps making the system linear and expressing it as in eq. 7. Moreover, the overall moment depends only on the roll angular velocity if the change of the atmospheric density $\rho$is neglected (since the height reached is not over a couple kilometers). Finally, the surface $S$ stands for the surface of the base of the rocket, and is constant.

$$I\ddot{\phi} + \frac{1}{2}\rho v C_{l_p}\dot{\phi}d^2 S = \frac{1}{2}\rho v^2 C_{l_0} S\, d + M_c \tag{9}$$

The resulting system is a second order system with real non-positives poles, a control input and a perturbation represented by the forcing aerodynamic moment.

### 5.2 Navigation

The IMU is capable of providing measurements of acceleration and angular velocity around the roll axis. To schedule the gains of the control law with respect to velocity and to provide the current roll angle, an integration of the measurements shall be performed on-board. The inertial acceleration $\dot{v_m}$ measurement can be integrated with the trapezium rule (eq. 10), as well as the roll angular velocity, which is also filtered by a complementary filter (eq. 11) : a roll angle measurement $\phi_{m_{i_{ACC}}}$ can also be obtained from the accelerometers and fused with the one obtained integrating angular velocity.

$$v_{m_i} = v_{m_{i-1}} + (\dot{v}_{m_{i-1}} + \dot{v}_{m_i})/2\ \Delta t \tag{10}$$

$$\phi_{m_i} = 0.98\ [\phi_{m_{i-1}} + (\dot{\phi_{m_{i-1}}} + \dot{\phi_{m_i}})/2\ \Delta t] + 0.02\ \phi_{m_{i_{ACC}}} \tag{11}$$

### 5.3 Control

#### 5.3.1 Control law design

Due to the inherent non-linear nature of cold gas actuators, a non-linear control law was developed.[2] The choice fell on a Schmitt trigger, i.e. a hysteresis to maintain the roll angle within a certain range around the given setpoint.
The input to the Schmitt trigger is the roll angle error, i.e. the difference between the desired angle $\phi_{ref}$ and the measured angle $\phi_m$. However, the presence of a limit cycle in relation to a certain upper threshold ($u_{on}$) of the trigger depends on the airspeed: below a certain airspeed, the limit cycle disappears. In particular, the limit speed is linked to the chosen threshold, but at this speed, the cycle is always present for the upper thresholds of lower value. Consequently, below the limit speed, a derivative gain $T_D$ applied to the measurement of the angular velocity of the roll is necessary to make the input control $u_{in}$ slightly greater in absolute value than the actual error and thus trigger the threshold in advance, an action necessary to compensate for the delay introduced by the actuators. In this way, the limit cycle presence is maintained.

$$u_{in} = \phi_{ref} - \phi_m - T_D\dot{\phi_m} \tag{12}$$

In addition to the upper threshold and the derivative gain, it is necessary to define a lower hysteresis threshold ($u_{off}$) to limit the activation frequency of the jets and to avoid unnecessary usage of the compressed air. As stated before, due to the intrinsic dependence of the aerodynamic moments on the flight speed, the threshold and gain values are adaptive in order to maintain the desired performance.
Once the Schmitt trigger has been defined, each input corresponds to an output equal to -1, 0 or 1, in order to eventually activate a pair of actuators: in particular, when $u_{out} = 1$, a negative control moment is commanded and when $u_{out} = 0$, the actuators are switched off. As there are two directions of activation, there are also two effective hystereses, with the same thresholds but of opposite sign, as visible in Fig. 6.

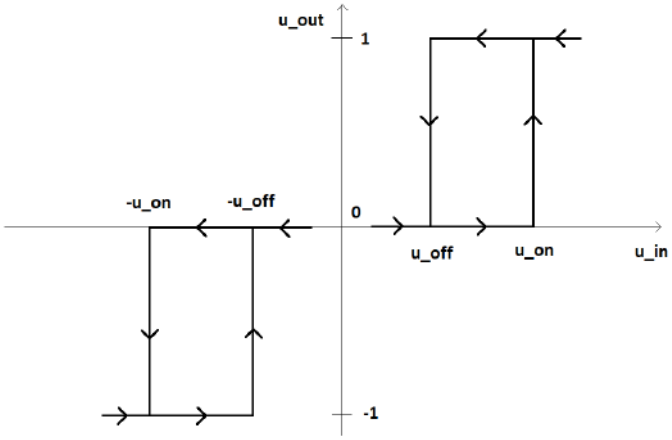


Figure 6: Schmitt trigger control logic

#### 5.3.2 Gains computation

The cold gas system put in place is limited in its activation capabilities : the solenoid valves governing the air flux through the nozzles have opening and closure transients. These transients can be taken into account as delays with a Pade' approximation of the first order, supposing the two transients of the same duration. After a change of variables, a first harmonic analysis can be performed taking into account the system in Fig. 8. The following set of variables substitutes the physical ones already presented, by performing a scaling based on the inertia $I$ and the control moment

$M_c$:

$$
\begin{aligned}
f &= \frac{1}{2}\rho v C_{l_p} d^2 S / I \\
M_0 &= \frac{1}{2}\rho v^2 C_{l_0} d S / M_{sat} \\
u_{sat} &= M_{sat} / I \\
K &= T_D \\
A_1 &= u_{off} / u_{sat} \\
A_2 &= u_{on} / u_{sat} \\
x_1 &= \phi \\
x_2 &= \dot{\phi}
\end{aligned}
$$

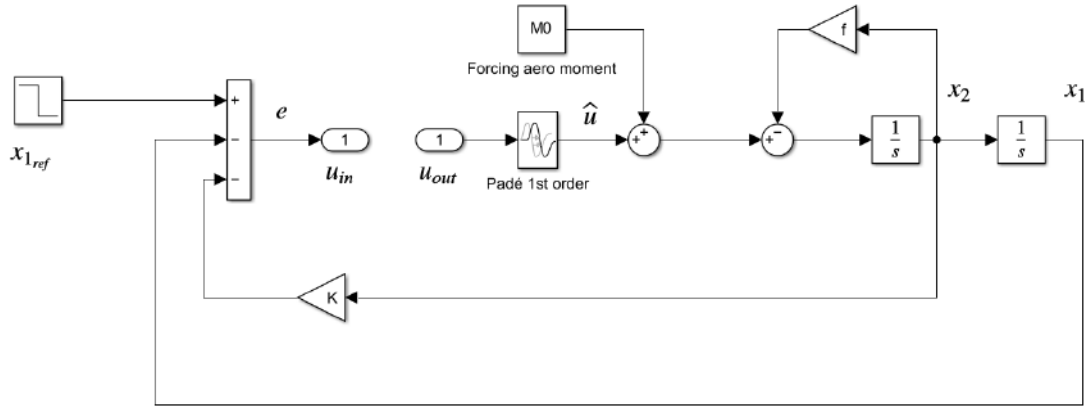


Figure 7: Simplified linear system with modified variables and parameters.

The first harmonic analysis applied to this system makes it easy to compute the frequency $\omega_c$ and amplitude $X_0$ of the limit cycle of $u_{in}$, which, for a small $K$, is very close in magnitude to $x_1$, the variable representing the roll angle. To represent the Schmitt Trigger as a Fourier series for the first harmonic analysis, the complex gain $N$ is defined in eq. 15 through the coefficients $a_1$ and $b_1$.

$$a_1(X_0) = 2/(\pi X_0)[(X_0^2 - A_2^2)^{1/2} + (X_0^2 - A_1^2)^{1/2}] \tag{13}$$

$$b_1(X_0) = -2/(\pi X_0)(A_2 - A_1) \tag{14}$$

$$N(X_0) = (a_1(X_0) + j\, b_1(X_0))/X_0 \tag{15}$$

The three parameters to be tuned are the thresholds $u_{off}$ and $u_{on}$ and the derivative gain $T_D$. The tuning is then performed following these steps:

- With the thresholds set to the same value and a null derivative gain, the velocity $v$ is increased until $v_1$, for which limit cycles disappear.
- The lower threshold $u_{off}$ is then chosen and $v$ is increased starting from the previously found value until $v_2$, for which limit cycles disappear.
- The derivative gain is then introduced for velocities lower than $v_1$ to avoid the appearance of limit cycles of large amplitude.

### 5.3.3 Case study : CERES experimental rocket

The law is here tuned basing on the aerodynamics and mass of the CERES experimental rocket from the Perseus project, having the characteristics in Tab. 1.

Table 1: Characteristics of CERES experimental rocket

| Variable | Value | Unit |
|---|---|---|
| $C_{l_0}$ | 0.08 | - |
| $C_{l_p}$ | 49.3811 | - |
| $\rho$ | 1.225 | $kg/m^3$ |
| $I$ | 0.2396 | $kg\ m^2$ |
| $M_c$ | 6.36 | N m |
| Valves switch time | 20 | ms |

A threshold $u_{on}$ of 3° was chosen as the maximum threshold evaluated, so as not to deviate too much from the set point during the control.

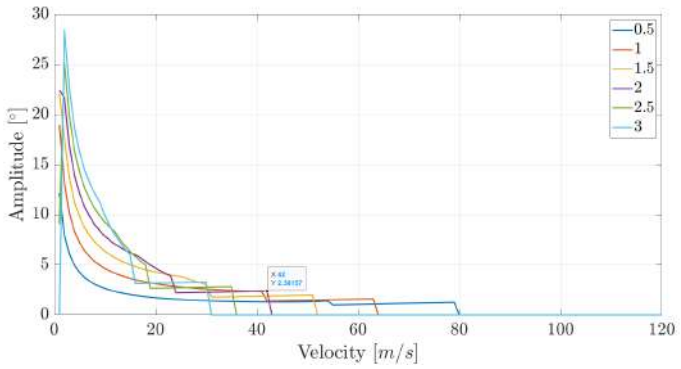


Figure 8: Analysis of upper threshold.

After defining the speed limits for each upper threshold, a threshold of 2° was chosen. This shows the disappearance of the limit cycle at a speed of 42 $m/s$ with an overshoot of 19 % (Fig. 8). To avoid the risk of falling into the limit cycle due to estimation errors and having excessive overshoots, this speed was increased by 5 %, thus passing into the zone where the limit cycle is not present. With only one threshold, actuators activate and deactivate as they cross it, with excessive frequency and for short activation periods. It is therefore preferable to introduce hysteresis via a lower threshold. The analysis was carried out by setting the upper threshold to 2° and varying the lower threshold and speed.

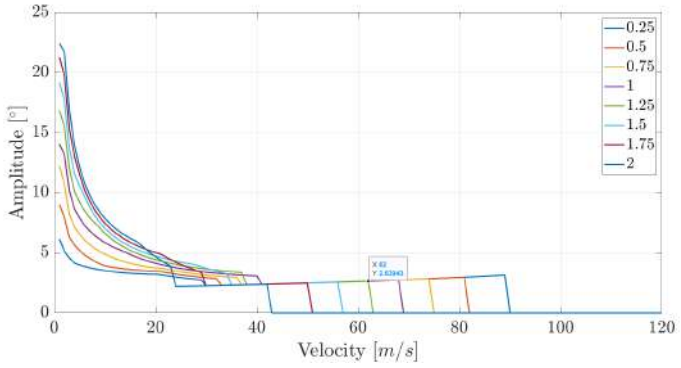


Figure 9: Analysis of lower threshold.

As Fig. 9 shows, as the lower threshold decreases, overshoot is amplified, so it is necessary to find a compromise between overshoot and activation frequency. Therefore, a lower threshold of 1.25° was chosen, which corresponds to

a limiting velocity of 62 $m/s$. The corresponding velocity was increased by 5 %, thus moving into the region where a limit cycle is not present.

For speeds below the upper threshold limit, a derivative gain is required to avoid a large amplitude limit cycle. Therefore, a zero speed analysis was performed by applying different derivative gains, obtaining the results of oscillation period and amplitude in Tab. 2.

Table 2: Performance with different derivative gains

| $\mathbf{T_D}$ $[ms]$ | **Amplitude** [°] | **Period** $[s]$ |
|---|---|---|
| 25 | 2.45 | 0.273 |
| 30 | 2 | 0.301 |
| 35 | 1.82 | 0.322 |
| 40 | 1.7 | 0.333 |
| 45 | 1.61 | 0.334 |

In the table, the values of $T_D$ have been considered starting from the first which does not lead to divergence. As can be seen, after 40 $ms$, there is no significant increase in the period, i.e. no decrease in the activation frequency, which is why a $T_D = 40$ $ms$ was chosen at zero speed.

Having defined the optimised thresholds for certain speeds and the maximum gain of the derivative at zero speed, it is possible to make them dependent on the speed of flight in order to optimise the control. A linear relationship is sufficient to link a lower threshold to each speed (up to the limit of the chosen lower threshold) and to obtain zero derivative gain at the limit speed of the chosen upper threshold. The resulting curves are visible in Fig. 10.

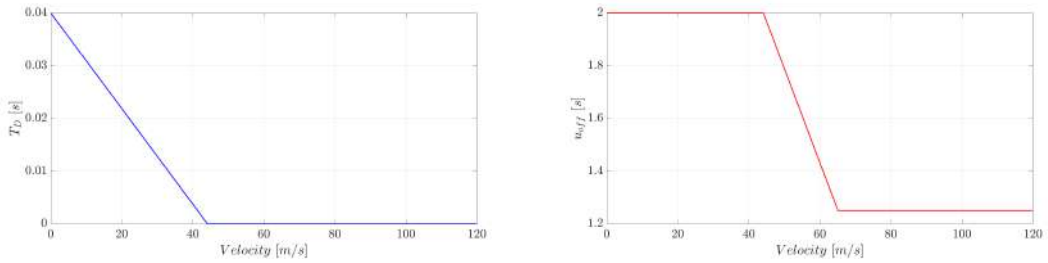


(a) $T_D$ (b) $u_{off}$

Figure 10: Derivative gain and lower threshold

## 6. Results

The control law has been tested on a test bench resembling the characteristics of the real experimental rocket in terms of inertia. In reality, characteristics such as the control moment magnitude and the switch time of the valves are different from the ones supposed when conceiving the control law. Thus, the following results compare the real data obtained from the controller card and a simulation based on the original control law applied to a physical system with the characteristics of the test bench in Table 3.

Table 3: Characteristics of test bench

| **Variable** | **Value** | **Unit** |
|---|---|---|
| $I$ | 0.29 | $kg\ m^2$ |
| $M_c$ | 3.6 | N m |
| Valves switch time | 30 | ms |

It shall be taken into account that the test is representative only of a specific case in which the velocity is null, due to the limitations of the test bench. The next figures (Figs. 11, 12 and 13) show the compared results in terms of roll angular velocity, roll angle and normalised control moment. As visible in Fig. 12, the allure of the limit cycle is

perturbed with respect to the simulated one, due to the approximations present in the physical system used to synthesise the control law. Overall, the result is satisfying and the real system results stable, with amplitude and frequency of the limit cycle comparable to the expected ones. Another important result is the robustness of the law, which is still valid for a test bench having different characteristics in inertia and control moment from the ones used for tuning.

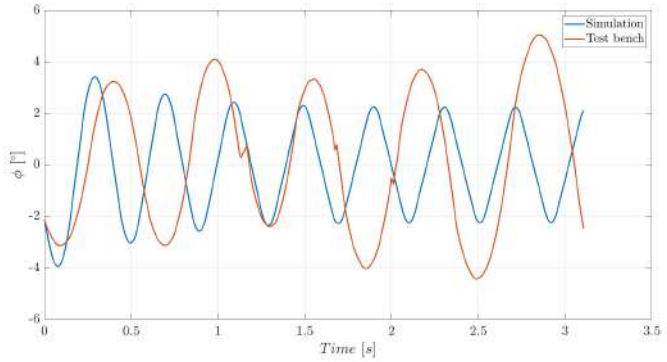


Figure 11: Evolution of roll angle over time, $I = 0.29\ kg\ m^2$

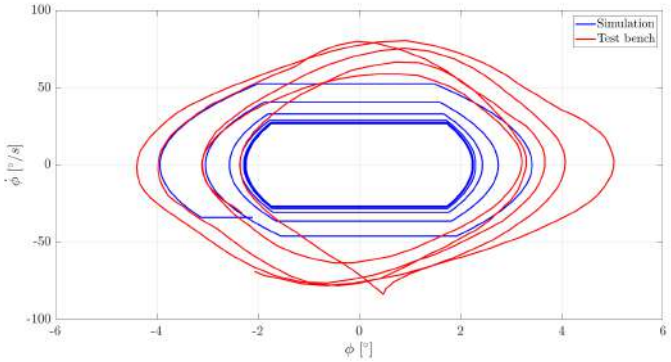


Figure 12: Phase plane, $I = 0.29\ kg\ m^2$

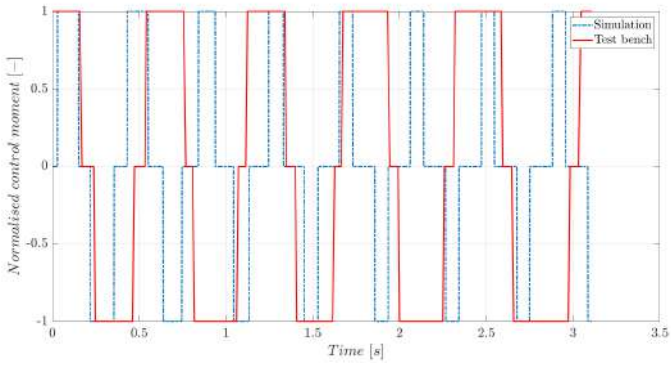


Figure 13: Normalised control moment over time, $I = 0.29\ kg\ m^2$

By changing the inertia of the test bench and bringing it up to 0.95 $kg\ m2$, it is possible to observe that the law is still valid (Figs. 14, 15 and 16).

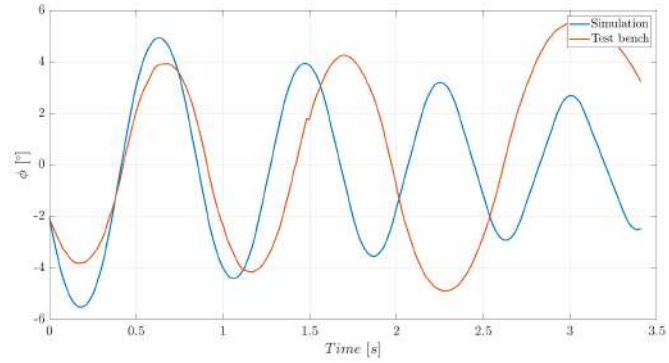


Figure 14: Evolution of roll angle over time, $I = 0.95\ kg\ m^2$

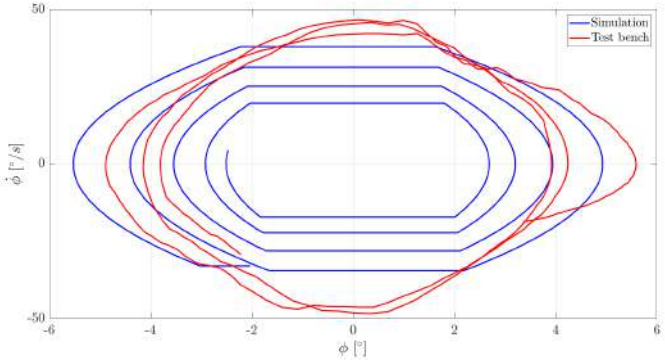


Figure 15: Phase plane, $I = 0.95\ kg\ m^2$

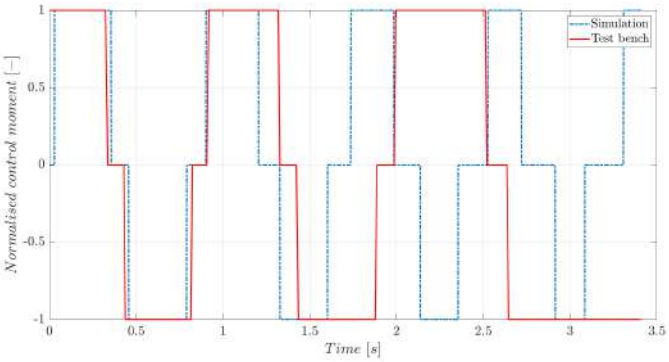


Figure 16: Normalised control moment over time, $I = 0.95\ kg\ m^2$

## 7. Conclusion

The pneumatic circuit alongside the mechanical extendable system provide, with a fast enough respond time, a sufficient moment. Thus the control law implemented within the electronic card shows good result for the capabilities of the system to control the roll angle of the rocket. The results of the tests suggest the need to ensure the robustness of the control law to counter all the discrepancies of the theoretical model from the real dynamics. The final step will be the launch of the rocket SERENDIPITY in July 2023, successor of CERES. It will show if the system is functional and efficient in a condition of high velocity, both for the aerodynamic moment and for the heavy stress that will be put on the extendable arms.

## 8. Acknowledgments

We would like to thank Mr. Jean Pierre Belmont for the help provided in the tuning of the control law and Mr. Timothée Grosbois-Favreau and all the PERSEUS team for managing the conception of the rocket.

## References

[1] Sighard F. Hoerner. *Fluid-Dynamic Drag : Practical Information on Aerodynamic Drag and Hydrodynamic Resistance*, volume 1. Sighard F. Hoerner, 1965.

[2] Shankar Sastry. *Nonlinear systems: analysis, stability, and control*, volume 10. Springer Science & Business Media, 2013.